 doi:10.20944/preprints202008.0580.v1

Original Research Article

The housekeeping transporter SLC25A44 bridges between the secondary metabolism and mitochondrial electron transfer chains

Behrooz Darbani

The Novo Nordisk Foundation Center for Biosustainability, Technical University of Denmark, 2800 Kgs. Lyngby, Denmark

Email: behroozdarbani@gmail.com, behdas@biosustain.dtu.dk, Tel.: +45-53 57 80 55

Abstract

The solute carrier family 25 (SLC25) participates in the transport of metabolites and cofactors across the membranes of mitochondria, plastids, peroxisomes, and endoplasmic reticulum. By calling for genomic blocks involved in adjacent metabolic reactions, this report introduces gene clusters of the *Slc*25 subfamily 44, stilbene and chalcone synthases, and subunits of the mitochondrial electron transfer complexes. The *Slc*25A44 gene was found ubiquitously expressed and transcriptionally co-regulated with energy metabolism genes in human, mouse, and *Arabidopsis thaliana*. The *Slc*25A44s also had no homozygous missense mutation and were highly conserved at intra-species level with the majority of polymorphism present in the non-coding regions. When expressed in oocytes, *AdSlc*25A44 from *Arachis duranensis* showed transport activity for the common precursors of flavonoids, stilbenoids, and ubiquinone. Accordingly, *Ad*SLC25A44 and its human orthologue *Hs*SLC25A44 elevated the production of *para*-coumaric, 4-aminobenzoic, and 4-hydroxybenzoic acids in *Saccharomyces cerevisiae* strains designed to produce *para*-coumaric acid via different pathways. Moreover, the engineered SLC25 subfamily specific signature, *i.e.,* *Ad*SLC25A44^{LWW206IQF}, had a stronger effect on *para*-coumaric acid secretion than the native variant. Importantly, the aerobic growth-rate of *S. cerevisiae* was significantly higher when expressing the *Ad*SLC25A44, *Hs*SLC25A44, or *Ad*SLC25A44^{LWW206IQF}. These results suggest that SLC25A44 is an essential mitochondrion-ER-nucleus zone transporter associated with metabolism of secondary metabolites and energy.

Keywords: Aminobenzoic acid, cinnamic acid, gene clusters, hydroxybenzoic acid, resveratrol, SLC25 subfamily 44, *para*-coumaric acid, ubiquinone

Introduction

Known as mitochondrial carriers, the SLC25 transporters (2.A.29) are only present in eukarya, as recently confirmed by genome-wide transportome analysis of 249 species[1]. On average, fungal and algal species have 35 members, plants have 65 members, and mammals have 54 members of SLC25 transporters[1]. The SLC25s are not restricted to the mitochondria and participate in the metabolite trafficking for ER, peroxisomes, and plastids[2–4]. The SLC25 transporters are critical for plastids and mitochondria and thereby for the metabolism of energy. Accordingly, the defective SLC25s are associated with multiple diseases in humans[5,6]. However, the function for nearly half of them is still unknown.

There is an increasing evidence for the biosynthetic gene clusters with non-biosynthetic transporter genes[7,8]. Accordingly, applying the genomic information is very promising approach to identify candidate transporters

which are a part of gene clusters[7,9]. Following the same approach, the flavonoid and stilbenoid biosynthetic pathway genes and the genes coding for subunits of mitochondrial electron transfer chains (ETC), such as ubiquinone oxidoreductases, were found as co-localized with *Slc*25A44. It was hypothesized that SLC25A44 may be transporting the common precursors of the ubiquinone which is the electron shuttle in ETC[10,11] and the secondary metabolites such as resveratrol[12]. This was further confirmed by the functional analyses of *Arachis* and human SLC25A44s in *Xenopus* oocytes and *S. cerevisiae*.

Results

Identification of the *Slc*25A44

Taking the advantage of gene clusters[7,9], a genome-wide investigation was performed on the neighboring genes for resveratrol synthase genes, which are responsible for the conversion of *para*-coumaric acid to resveratrol. A gene cluster harboring resveratrol synthases, chalcone synthases, mitochondrial complex I subunit *Nduf*A12, quinone oxidoreductase, and *Slc*25A44 genes was found in the genomes of peanut (*Arachis hypogaea*) and its diploid ancestors (*A. duranensis* and *A. ipaensis*) that naturally produce resveratrol (Fig. 1a). The transporter proteins *Ad*SLC25A44, *Ai*SLC25A44, and *Ah*SLC25A44 were 99% identical. In grape (*Vitis vinifera*) and other plant species from Fabaceae, Cucurbitaceae, and Rosaceae families, *Slc*25A44 co-localized only with the genes coding for the mitochondrial ETC subunits (Table 1). Co-localization of the flavonoid biosynthetic genes (resveratrol synthases, chalcone synthases, and 4-coumarate-CoA ligases) and ETC subunit coding genes was also observed on different chromosomes of grape and four species from Fabaceae (Table 1). In contrast, there was not any similar genomic arrangement in the plant species *Oryza sativa* (Poaceae), *Gossypium hirsutum* (Malvaceae), *Arabidopsis thaliana*, *Brassica oleracea*, and *Capsella rubella* (Brassicaceae). Evolving of such gene clusters were also investigated in nine animal species including *Homo sapiens, Mus musculus, Gorilla gorilla gorilla, Bos taurus, Xenopus laevis, Drosophila melanogaster, Cimex lectularius, Halyomorpha halys, and Caenorhabditis elegans*. The *Slc*25A44 was found adjacent to the mitochondrial complex III subunit UQCRQ coding gene only in the genome of the insect *H. halys* (Table 1). The existence of gene clusters with different combinations of genes, all implicated in the same metabolic pathway, is consistent with the convergent evolution of gene clusters[13].

The co-upregulation of *Slc*25A44 and the resveratrol biosynthesis pathway genes of phenylalanine ammonia-lyase (*Pal*) and resveratrol synthases were further noticed in grape berries transcriptome data[14]. Therefore, co-expression and pathway enrichment analyses were applied for *Slc*25A44 using the *A. thaliana* and mouse public data. Co-expression analysis for *AtSlc*25A44 found 368 genes mainly associated with biotic and abiotic stress responses, but also genes involved in the energy metabolism, such as oxoglutarate

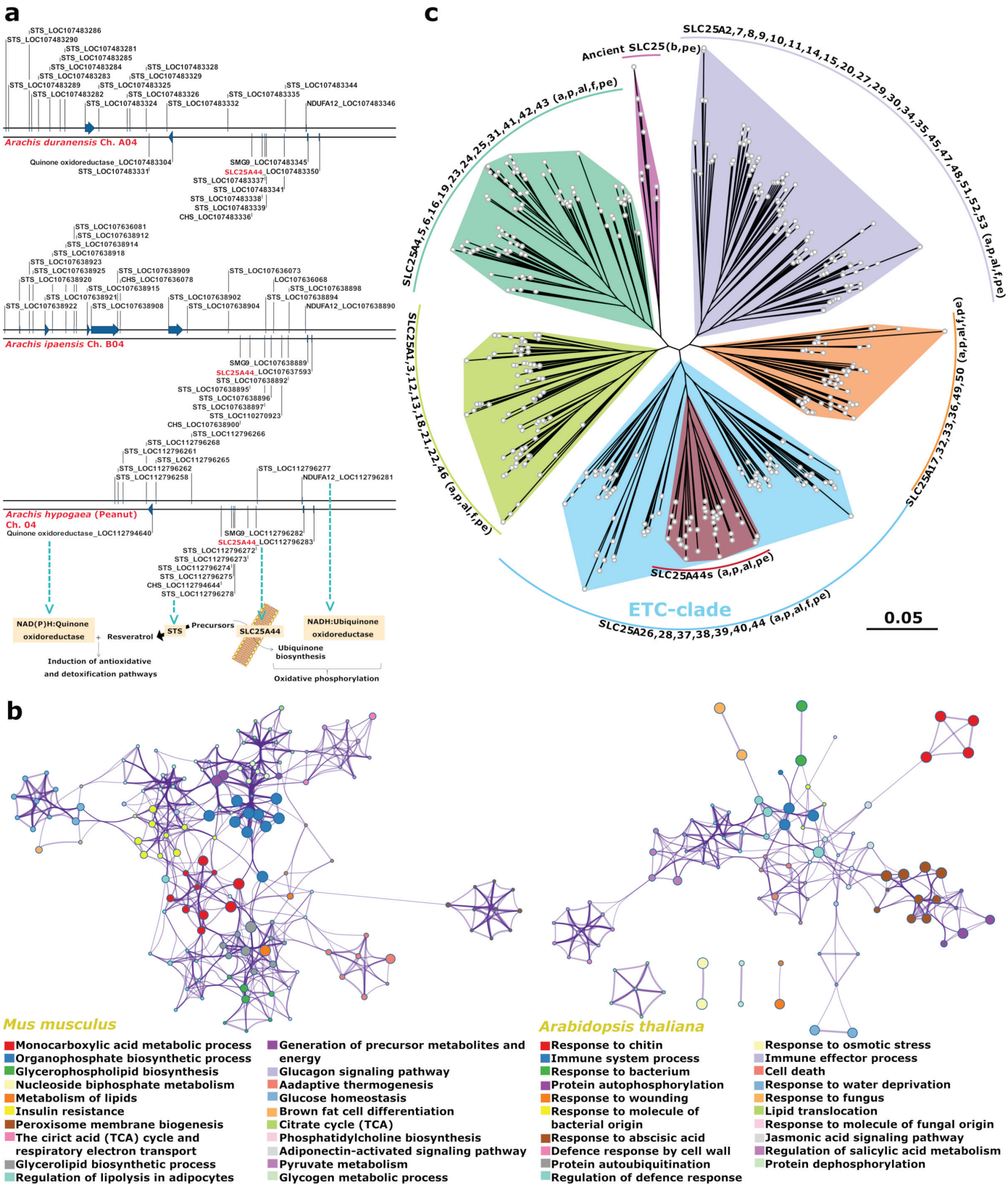

Fig. 1: Identification of SLC25A44 as a candidate transporter for the common precursors of ubiquinone and resveratrol. a, The identified gene clusters in peanut and its ancestors *A. ipaensis* and *A. duranensis*. The metabolic relation among the genes is shown. **b,** Metabolic pathway enrichment for the genes co-expressed with *Slc*25A44. **c,** The phylogenetic tree of mitochondrial carriers. The tree includes SLC25 members from four primitive eukaryotes, four fungal species, two animals, one plant and one algal species, ancient SLC25 members from five bacterial species, and finally members of SLC25A44 from additional 18 animals and seven plant and algal species. See Table 1 and Extended Data Table 2 for the species names and accession number of sequences. The clades are labeled by letters "a" for animal, "p" for plant, "f" for fungi, "pe" for primitive eukaryotes, and "b" for bacteria when there is at least one representative transporter member from the corresponding domains of life. CHS: chalcone synthase, ETC: electron transfer chains, NDUF: NADH ubiquinone oxidoreductase, STS: resveratrol synthase.

Preprints (www.preprints.org) | NOT PEER-REVIEWED | Posted: 26 August 2020 doi:10.20944/preprints202008.0580.v1

dehydrogenase, dihydrolipoamide succinyltransferase, pyruvate kinase, and NAD(P)H dehydrogenase B2 (Fig. 1b, Extended Data Table 1). The mouse *MmSlc*25A44 was co-expressed with 247 genes mainly implicated in energy metabolism, *e.g.*, glucose transporter *Slc*2A4, citrate synthase, mitochondrial citrate transporter *Slc*25A1, and ETC subunit coding genes (Fig. 1b, Extended Data Table 1).

Table 1. Identified genomic co-localizations

Species/Family	*Chromosome or Contig*	*Co-localized Loci with GenBank accession numbers*
Vitis vinifera/Vitaceae	Ch.14 Ch.16 Ch.13	***Slc*25A44** (XP_010660575.1), ***Ndufa*4** (XP_002281305.1) ***4Cl*2** (XP_002274994.1), ***Ndufs*6** (XP_002276949.1), ***Smg*9** (XP_010662114.1), ***Ndufa*12** (XP_002276966.1), ***Cox*11** (XP_002277478.1) ***Slc*25A38** (XP_002277407.1), ***Atp*5H/*ATP synthase* d** (XP_002277452.1), ***Tim*14-1** (XP_002277365.1)
Cajanus cajan/Fabaceae	Ch.8 NW_017984070.1 Ch.2	***Slc*25A44** (XP_020221994.1), ***Lyrm*** (XP_020221999.1) ***Chalcone synthase*** (XP_020230031.1), ***Ndufa*12** (XP_020230179.1), ***Smg*9** (XP_020230144.1), ***4Cl*2** (XP_020230139.1) ***Slc*25A38** (XP_020234579.1), ***Atp*5H/*ATP synthase* d** (XP_020202519.1)
Glycine max/Fabaceae	Ch.9 Ch.11 Ch.20	***Slc*25A44** (XP_025979445.1), ***Lyrm*** (XP_025979447.1) ***4Cl*3** (NP_001237270.1), ***Smg*9** (XP_014619235.1); ***Ndufa*12** (NP_001235085.1), ***Chalcone synthase*** (NP_001304585.2) ***Slc*25A38** (XP_003556216.1), ***Atp*5H/*ATP synthase* d** (NP_001235072.1)
Phaseolus vulgaris/Fabaceae	Ch.6 Ch.2 Ch.4	***Slc*25A44** (XP_007147410.1), ***Lyrm*** (XP_007147403.1) ***Chalcone synthase*** (XP_007157053.1), ***Ndufa*12** (XP_007157055.1), ***Smg*9** (XP_007157056.1), ***4Cl*** (XP_007157067.1) ***Slc*25A38** (XP_007143676.1), ***Atp*5H/*ATP synthase* d** (XP_007143675.1)
Vigna radiata/Fabaceae	Ch.10 Ch.11 Ch.8	***Slc*25A44** (XP_022642859.1), ***Lyrm*** (XP_014517948.1) ***4Cl*2** (XP_014521169.1), ***Smg*9** (XP_014519466), ***Ndufa*12** (XP_014519966.1, XP_022643154.1), ***Chalcone synthase*** (XP_014520574.1) ***Slc*25A38** (XP_014514167.1), ***Atp*5H/*ATP synthase* d** (XP_014511180.1)
Cicer arietinum/Fabaceae	Ch.1 Ch.8 Ch.4	***Slc*25A44** (XP_027189994.1), ***Lyrm*** (XP_004486516.1) ***4Cl*2** (XP_004511423.1), ***Smg*9** (XP_004511426.1), ***Chalcone synthase*** (XP_012574354.1) ***Slc*25A38** (XP_004496329.1), ***Atp*5H/*ATP synthase* d** (XP_004496331.1)
Medicago truncatula/ Fabaceae	Ch.2 Ch.5 Ch.1	***Slc*25A44** (XP_024632094.1), ***Lyrm*** (XP_003594632.1) ***4Cl*2** (XP_003610843.1), ***Smg*9** (XP_003610849.1), ***Chalcone synthase*** (XP_013453346.1) ***Slc*25A38** (XP_003591971.1), ***Atp*5H/*ATP synthase* d** (XP_003591975.1)
Lupinus angustifolius/ Fabaceae	Ch.16 Ch.17 Ch.20	***Slc*25A44** (XP_019418829.1), ***Lyrm*** (XP_019418830.1) ***Smg*9** (XP_019420313.1), ***Chalcone synthase*** (XP_019420991.1) ***Slc*25A38** (XP_019427565.1), ***Atp*5H/*ATP synthase* d** (XP_019427572.1)
Cucumis sativus/ Cucurbitaceae	Ch.3 Ch.5	***Slc*25A44** (XP_004147664.2), ***Lyrm*** (XP_004147626.1) ***Slc*25A38** (XP_004142487.1), ***Atp*5H/*ATP synthase* d** (XP_004142418.1), ***Tim*14-1** (XP_004142436.1)
Prunus persica/Rosaceae	Ch.1 Ch.2	***Slc*25A44** (XP_020410285.1), ***Lyrm*** (XP_020410759.1) ***Slc*25A38** (XP_007220258.1), ***Atp*5H/*ATP synthase* d** (XP_007218513.1), ***Tim*14-1** (XP_007219829.1)
Homo sapiens/Hominidae	Ch.1 Ch.10	***Slc*25A44** (NP_001273113.1), ***Smg*5** (NP_001310543.1) ***Slc*25A28** (XP_011538541.1), ***Cox*15** (NP_510870.1), ***Cut*C** (NP_057044.2)
Gorilla gorilla gorilla/Hominidae	Ch.1 Ch.10	***Slc*25A44** (XP_004026998.1), ***Smg*5** (XP_018879956.1) ***Slc*25A28** (XP_018890384.2), ***Cox*15** (XP_004049980.3), ***Cut*C** (XP_030870896.1)
Mus musculus/Muridae	Ch.3 Ch.19	***Slc*25A44** (NP_001139348.1), ***Smg*5** (NP_839977.2) ***Slc*25A28** (NP_660138.1), ***Cox*15** (NP_659123.2), ***Cut*C** (NP_001107034.1)
Bos Taurus/Bovidae	Ch.3 Ch.26	***Slc*25A44** (NP_001071325.1), ***Smg*5** (NP_001077148.1) ***Slc*25A28** (NP_001192481.1), ***Cox*15** (NP_001070329.1), ***Cut*C** (NP_001193825.1)
Xenopus laevis/Pipidae	Ch. 8S Ch. 7S	***Slc*25A44** (NP_001090232.1), ***Smg*5** (XP_018089021.1) ***Slc*25A28** (XP_018083007.1, NP_001086329.1), ***ATP Synthase* 6v0e2** (NP_001165047.1), ***Cox*15** (XP_018083005.1)
Halyomorpha halys/ Pentatomidae	NW_020110602.1	***Slc*25A44** (XP_014285646.1), ***Uqcrq*** (Complex III Subunit, XP_024215595.1)
Saccharomyces cerevisiae	Ch.16	***Agc*1** (Aspartate-glutamate carrier, YPR021C), ***Atp*20** (F1-F0 ATPase assembly protein, YPR020W)
Pichia membranifaciens	NW_017566982.1	***Agc*1** like (XP_019020020.1), ***Sqr*** (Complex II subunit, XP_019020021.1)
Schizosaccharomyces pombe	Ch.1	***Agc*1** like (NP_593068.1), ***Atp*10** (F1-F0 ATPase assembly protein, NP_593071.1)
Candida tenuis	NW_006281231.1	***Agc*1** like (XP_006684445.1), ***Ndufa*8** (XP_006684447.1)
Scheffersomyces stipites	Ch.1	***Agc*1** like (XP_001387183.2), ***Cox*19** (Complex IV chaperone, XP_001386938.2)

4CL: 4-coumarate-CoA ligase, COX: Cytochrome C Oxidase/Complex IV chaperone, CUTC: Copper homeostasis protein, LYRM: LYR motif containing protein/Complex I subunit, NDUF: NADH ubiquinone oxidoreductase/Complex I subunit, SLC25A44: Solute carrier family 25 subfamily 44, SQR: Succinate quinone oxidoreductase/Complex II subunit, UQCRQ: Ubiquinol-cytochrome C reductase/Complex III Subunit.

*Slc*25A44 is a highly conserved housekeeping transporter gene

The SLC25 family has diverged massively, and in humans, it consists of 53 subfamilies. The bacterial ancient SLC25 transporters were recently proposed as the evolutionary origin for the modern eukaryotic SLC25s[1]. In agreement, primitive eukaryotes code for close homologs of the ancient bacterial SLC25s (Fig. 1c). Phylogenetic analysis identified five major clades of modern SLC25s (Fig. 1c). The SLC25A44 was in a clade with the S-adenosylmethionine transporter SLC25A26[15], the iron transporters of SLC25A28 and A37[16], and the uncharacterized transporters of SLC25A38, A39, and A40 (Fig. 1c). The SLC25A38 and A39 have been reported to be associated with heme biosynthesis[17,18]. This clade was called ETC-clade due to the

Preprints (www.preprints.org) | NOT PEER-REVIEWED | Posted: 26 August 2020 doi:10.20944/preprints202008.0580.v1

structural and functional dependency of ETC on the S-adenosylmethionine[19], iron, and heme[20–22]. Interestingly, the *Slc*25A28 and *Slc*25A38 genes also co-localized with the genes coding for ETC subunits, ATP synthase subunits, and the copper homeostasis protein CUTC (Table 1). Moreover, the *Slc*25A44 gene was found in animals, plants, algae, and primitive eukaryotes (Fig. 1c). In contrast, there was no clear fungal homolog of SLC25A44 and thereby, highly diversified orthologues are conceivably functioning in fungi (Fig. 1c, Extended Data Fig. 1a). The yeast *Sc*AGC1 was the most immediate blast hit for SLC25A44 members (Extended Data Fig. 1b). The *Agc*1 also co-localized with the genes coding for mitochondrial respiratory subunits in different fungal species (Table 1). Further analyses identified a conserved three-amino acid signature (V/I/L/AWW) for SLC25A44s (Fig. 2a). This signature was distinguishable among the phylogenetic sub-clusters of the ETC-clade (Fig. 1c, 2a). The signature is situated onto the cytosolic face of transport cavity at the C–terminal end of transmembrane helix 4 (Fig. 2b).

The inspection of human proteome[23] revealed ubiquitous expression of *Hs*SLC25A44 with highest levels in brain, kidney, and liver (Extended Data Fig. 2). Analyzing the *A. thaliana* proteome[24] and transcriptome data[25] also revealed the constitutive expression of *At*Slc25A44 at levels similar to the housekeeping genes *Ubc*9 and *Gapdh* across hundreds of different conditions and tissues (Extended Data Fig. 3a–g). In addition, *Slc*25A44 was found highly conserved at the intra-species level with the majority of polymorphism in the non-coding regions (Fig. 2c). There was no missense mutation for *Slc*25A44 in different lines of *A. thaliana*, which is a self-fertilizing homozygote plant (Fig. 2c). In addition, the human *Slc*25A44 had only 3% of the variants within the coding regions; less than 0.8% were missense variants, all as very low-frequent and heterozygous-only SNPs (Fig. 2c). Similar polymorphism patterns were also observed for the mouse and rice *Slc*25A44 genes (Extended Data Table 3). The ubiquitous expression and high levels of intra-species conservation indicate that SLC25A44 is essential in higher eukaryotes.

Functional characterization of *AdSlc*25A44 in *Xenopus oocytes*

The *AdSlc*25A44 was expressed in *X. laevis* oocytes for functional analysis. The heterologous vacuolar and mitochondrial transporters are expressed, at least partially, in the plasma membrane of oocytes due to the very high-level translational capacity of oocytes and this allows for their characterization[7,9,26]. For the export assay, a solution consisting of resveratrol and *para*-coumaric acid was injected into the oocytes to a final intracellular concentration of ca. 2 mM each and the exported compounds into the Kulori buffer were quantified after 3.5 hours. The expression of *AdSlc*25A44 had no significant efflux activity for resveratrol and *para*-coumaric acid (Fig. 2d). In contrast, the import assay with Kulori buffer containing resveratrol and *para*-coumaric acid (0.2 mM each) showed *para*-coumaric acid transport activity for *AdSlc*25A44. Here, oocytes expressing *AdSlc*25A44 contained 14% more *para*-coumaric acid than the control oocytes with no heterologous transporter ($p = 9.6 \times 10^{-3}$, Fig. 2e). *AdSlc*25A44 was also examined for the import of cinnamic and 4-aminobenzoic acids and similar transport patterns were found (Fig. 2e, f). Oocytes expressing

*Ad*Slc25A44 had 35% ($p = 5.4 \times 10^{-3}$) and 20% ($p = 2.7 \times 10^{-3}$) higher intracellular levels of cinnamic and 4-aminobenzoic acids, respectively (Fig. 2f). There was no significant resveratrol-influx activity for *Ad*Slc25A44 (Fig. 2e). The lack of export activity could be explained due to the absence of a co-substrate in the buffer and the conceivable antiport activity, which is a common mechanism for the SLC25 members[27].

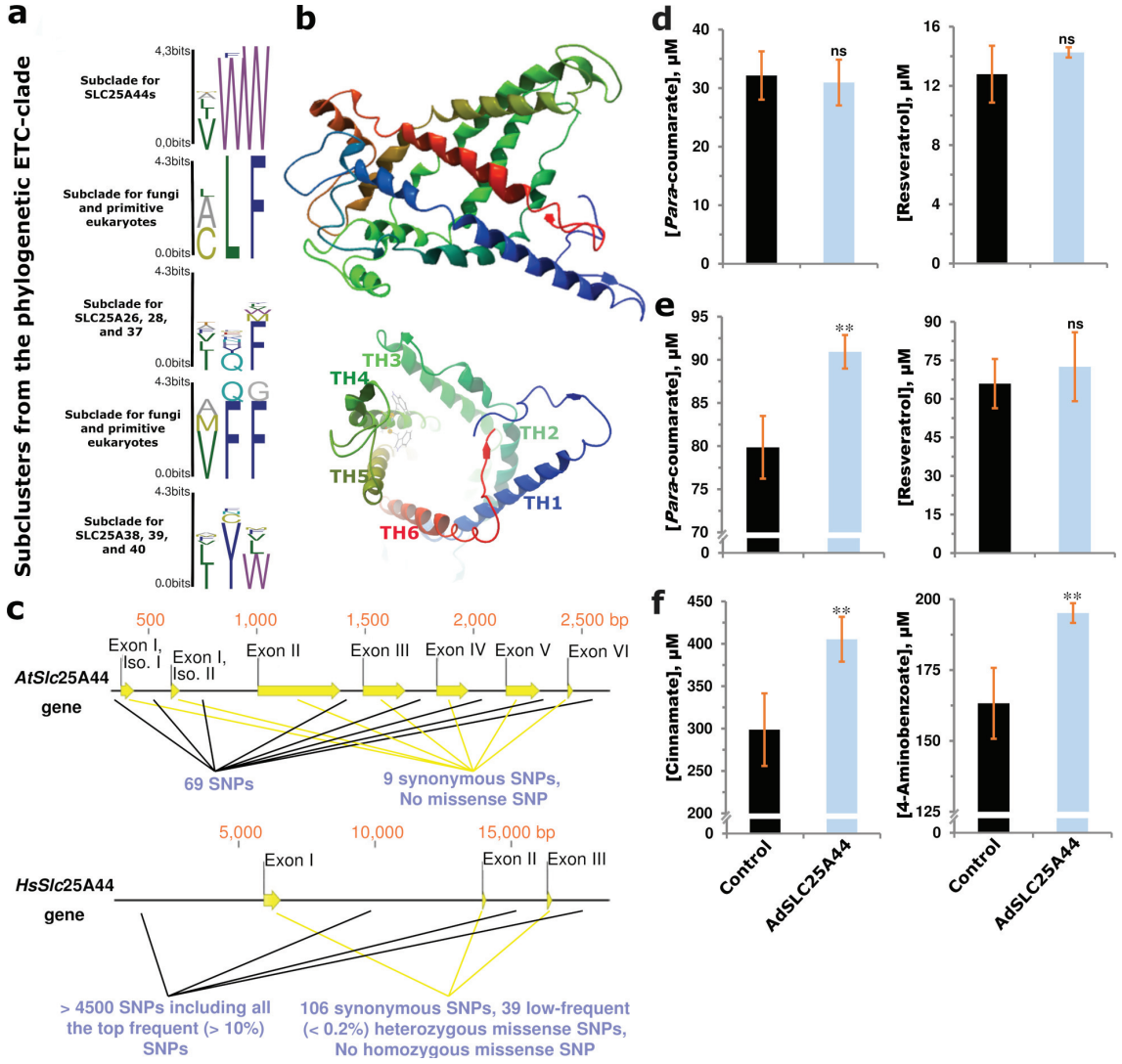

Fig. 2: The highly conserved *Slc*25A44 gene has transport activity when expressed in *X. laevis* oocytes. a, The conserved three-amino acid signature in SLC25A44s and four other subclades within the phylogenetic ETC-clade. **b,** The predicted whole and cytosolic face structure of the *Ad*SLC25A44. Transmembrane helices (TH) and conserved tryptophan residues on TH4 are illustrated. **c,** The structure of locus and polymorphism distribution for *Arabidopsis* and human *Slc*25A44s. **d-f,** Functional transport studies by expressing *Ad*Slc25A44 in oocytes. **d,** Export assay: resveratrol and *para*-coumaric acid were injected into the oocytes and were quantified in the medium after 210 minutes. **e, f,** Import assay: resveratrol and *para*-coumaric acid **(e)** or cinnamic and 4-aminobanzoic acids **(f)** were added into the medium and intracellular levels of these compounds in oocytes were quantified after 210 minutes. **d-f,** Bars represent mean ± Std. n = 3-4 biological independent samples each with 20 (**d**) or 30 (**e, f**) oocytes. The two-tailed Student's t-test was used to find the significant transport activities at 1% level (marked by two asterisks) when compared to the control with no heterologous expression.

Preprints (www.preprints.org) | NOT PEER-REVIEWED | Posted: 26 August 2020 doi:10.20944/preprints202008.0580.v1

SLC25A44 localized onto the mitochondria, ER, and nucleus of yeast and had impact on the production of *para*-coumaric, 4-aminobenzoic, and 4-hydroxybenzoic acids

The human SLC25A44 has previously been mapped on mitochondrion, ER, and nucleus[23]. To examine the localization of *Ad*SLC25A44, a C–terminal fused GFP version of *Ad*SLC25A44 was expressed in *S. cerevisiae*. The observed subcellular localization pattern (Fig. 3a) was similar to the previously reported yeast mitochondrial, ER, and nucleus membrane proteins such as CTP1, OXA1, YHM2, APQ12, ERD2, and BRR1[28]. For functional analysis of SLC25A44 in yeast, two different *S. cerevisiae* strains were built for *para*-coumaric acid production *via* different pathways. The chassis strain had knockouts of the phenylpyruvate and pyruvate decarboxylases (*Δaro*10, *Δpdc*5) to decrease the catabolism[29]. A strain called PAL and was designed to produce *para*-coumaric acid from phenylalanine. As reported previously[29], the *A. thaliana* genes coding for phenylalanine ammonia-lyase (*AtPal*2), cytochrome P450 reductase (*AtAtr*2), and cinnamic acid hydroxylase (*AtC4H*) were expressed and the native cytochrome b5 *ScCyb5* was overexpressed in the PAL strain. The expression of *AdSlc*25A44 in the PAL strain reduced the extracellular titers and specific yield of *para*-coumaric acid by 15% ($p = 3 \times 10^{-4}$) and 19% ($p = 3 \times 10^{-5}$), respectively (Fig. 3b). The production of related shikimate pathway intermediates including cinnamic, 4-aminobenzoic, and 4-hydroxybenzoic acids[30,31] were additionally examined. The expression of *AdSlc*25A44 resulted in lower extracellular levels of 4-hydroxybenzoic acid and 4-aminobenzoic acid. The titer and specific yield decreased up to 23% ($p = 9.6 \times 10^{-6}$) and 27% ($p = 1.9 \times 10^{-6}$) for 4-hydroxybenzoic acid and up to 33% ($p = 4.9 \times 10^{-2}$) and 36% ($p = 3.1 \times 10^{-2}$) for 4-aminobenzoic acid, respectively (Fig. 3b). There was no export for cinnamic acid from the PAL strain. The *AdSlc*25A44 was further expressed in a second yeast strain called TAL, which was designed for the biosynthesis of tyrosine-derived *para*-coumaric acid. The TAL strain was engineered by expression of the feedback-resistant genes $Aro4^{fbr}$ and $Aro7^{fbr}$ to boost the biosynthesis of aromatic amino acids[32] and by the expression of tyrosine ammonia-lyase (*FjTal*) from *Flavobacterium johnsoniae*. In the TAL strain, *AdSlc*25A44 improved the *para*-coumaric acid extracellular titer and specific yield by 18% ($p = 2 \times 10^{-6}$) and 19% ($p = 1.5 \times 10^{-6}$), respectively (Fig. 3c). However, the expression of *AdSlc*25A44 decreased the extracellular titer and specific yield of 4-hydroxybenzoic acid by 9% ($p = 1.8 \times 10^{-4}$) and 8% ($p = 4.6 \times 10^{-4}$), respectively (Fig. 3c). Here, *AdSlc*25A44 had no significant effect on the extracellular level of 4-aminobenzoic acid (Fig. 3c).

To examine whether these transport activities are common for SLC25A44s, the human *HsSlc*25A44 was expressed in the PAL and TAL yeast strains. The expression of *HsSlc*25A44 had a similar effect as the expression of *AdSlc*25A44 in the TAL strain. Here, the titer and specific yield of *para*-coumaric acid increased by 6% ($p = 1.6 \times 10^{-2}$) and 8% ($p = 4 \times 10^{-2}$), respectively (Fig. 3c). In contrast to the *AdSlc*25A44, the expression of *HsSlc*25A44 in the PAL strain improved the titers and specific yields of *para*-coumaric acid up to 6% ($p = 7 \times 10^{-3}$) and 30% ($p = 6 \times 10^{-6}$), 4-hydroxybenzoic acid up to 7% ($p = 1.6 \times 10^{-2}$) and

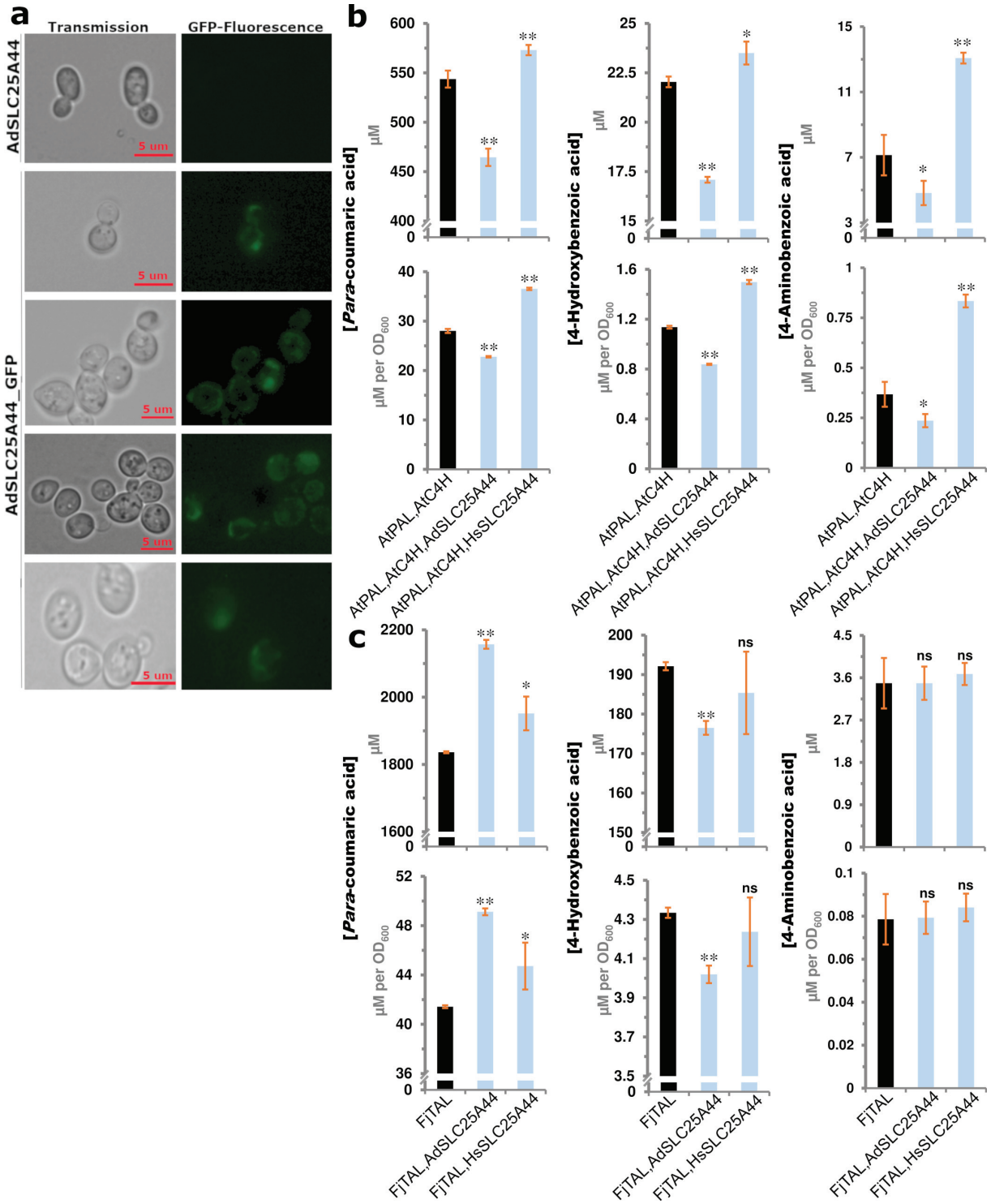

Fig. 3: The transport activities of *Ad*SLC25A44 and *Hs*SLC25A44 in *S. cerevisiae*. a, Subcellular localization of *Ad*SLC25A44_GFP in yeast. **b, c,** *Para*-coumarate, 4-aminobenzoate, and 4-hydroxybenzoate concentrations in the fermentation broth after 72 hours growth of the yeast strains producing *para*-coumaric acid from phenylalanine using the enzymes PAL and C4H **(b)** or from tyrosine using the enzyme TAL **(c)**. Bars represent mean ± Std. n = 3 biological independent samples. The two-tailed Student's t-test was used to compare the strains with and without the heterologous transporters. The significant events at 5% and 1% levels are labeled by one and two asterisks, respectively. C4H: Cinnamic acid hydroxylase, PAL: Phenylalanine ammonia-lyase, TAL: Tyrosine ammonia-lyase.

Preprints (www.preprints.org) | NOT PEER-REVIEWED | Posted: 26 August 2020 doi:10.20944/preprints202008.0580.v1

32% (p = 6.5 × 10^{-6}), and 4-aminobenzoic acid up to 83% (p = 1 × 10^{-3}) and 127% (p = 3 × 10^{-4}), respectively, in the fermentation broth (Fig. 3b). Overall, the transporters had similar effects except *Ad*SLC25-44 when it was expressed in PAL strain. This difference could be attributed to the interactions of *para*-coumaric acid biosynthesis in ER (PAL strain) or cytosol (TAL strain)[33] with the expected different distribution rates of *Ad*SLC25A44 and *Hs*SLC25A44 among mitochondria, ER, and nucleus.

Transporter engineering towards higher production of *para*-courmaric acid

Here, the focus was on the identified conserved motif in the cytosolic face of SLC25A44 (Fig. 2a, b). The VWW residues in *Hs*SLC25A44 occupy a smaller space than the LWW residues of *Ad*SLC25A44 due to the short side chain of valine. The corresponding residues in human ADP/ATP antiporter (SLC25A6) are AYF, all with smaller side chains. The LWW residues of the *Ad*SLC25A44 were then mutated into the IQF with smaller side chains. The IQF signature is also exist in the *Arabidopsis* plastid S-adenosylmethionine/S-adenosylhomocysteine antiporter (SLC25A26), which is the most immediate neighbor of SLC25A44 within the ETC-clade (Fig. 1c, 2a). The expression of *Ad*SLC25A44^{LWW206IQF} in the PAL and TAL yeast strains resulted in higher extracellular levels of *para*-courmaric acid (Fig. 4a, b). *Para*-coumaric acid is a valuable chemical building block and a precursor of flavonoids and stilbenoids[32]. The expression of SLC25A44^{LWW206IQF} in PAL strain improved the titer and specific yield of *para*-coumaric acid by 46% (p = 2.1 × 10^{-16}) and 18% (p = 3.6 × 10^{-10}), respectively (Fig. 4a). The titer and specific yield of *para*-coumaric acid also increased by 19% (p = 6.1 × 10^{-12}) and 27% (p = 1.2 × 10^{-12}), respectively, in the TAL strain expressing SLC25A44^{LWW206IQF} (Fig. 4b). Furthermore, the expression of SLC25A44^{LWW206IQF} enhanced the production of 4-hydroxybenzoic acid in the PAL (83%, p = 4.2 × 10^{-9}) and TAL (20%, p = 5.8 × 10^{-6}) strains (Fig. 4a, b). The production of 4-aminobenzoic acid was improved only in the PAL strain (Fig. 4a, b). Importantly, the expression of the SLC25A44 transporters not only enhanced the production but also improved the growth rate of yeast PAL and TAL strains (Fig. 4c).

Discussion

Here, the genomic positional information, which has been shaped by the evolutionary preference for the co-segregation of genes within gene clusters[7,13], have been employed to identify the *Slc*25A44 transporter gene. The *Slc*25A44 transporter gene found adjacent to the genes coding for resveratrol synthases, chalcone synthases, and subunits of mitochondrial ETC in different plant and animal species (Fig. 1, Table 1). Phylogenetic, polymorphism, and co-expression analyses together with functional transport studies uncovered the function of SLC25A44 as a transporter for the common precursors of ubiquinone, stilbenoids, and flavonoids (Fig. 1–4). The SLC25A44 thus links the primary energy metabolism to the secondary metabolism.

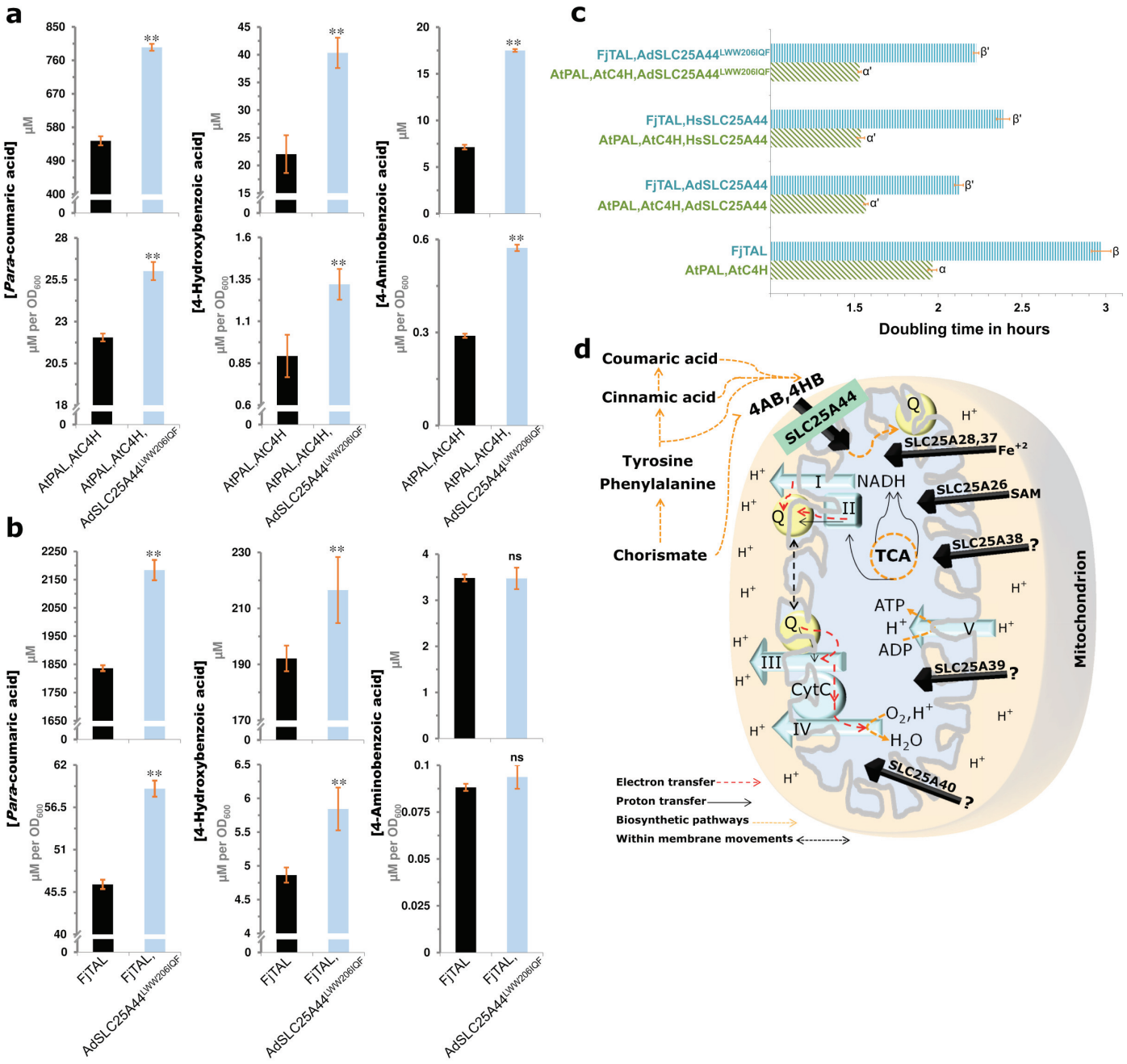

Fig. 4: The SLC25A44 is a transporter of ubiquinone precursors with potential to boost the bio-based production of *para*-coumaric acid. a, b, The effect of *Ad*SLC25A44^{LWW206IQF} expression on the production rate of *para*-coumaric, 4-hydroxybenzoic, and 4-aminobenzoic acids in both of the yeast PAL and TAL strains. Bars represent mean ± Std. n = 6-9 biological independent samples. The two-tailed Student's t-test was used to compare the strains with and without *Ad*SLC25A44^{LWW206IQF}. The significant events at 1% level are marked by two asterisks. **c**, Logarithmic cell growth was measured spectrophotometrically at A_{600} nm. Significant differences, *ie.*, α *vs* α′ and β *vs* β′ ($p = 10^{-4}$), were determined through one-way ANOVA followed by Least Significant Difference test. Bars represent mean ± Std. n = 3 biological independent samples. **d,** A simplistic roadmap for the involvement of SLC25A44 and the other transporter members of ETC-clade in the mitochondrial electron transfer chains. 4HB: 4-hydroxybenzoate, 4AB: 4-aminobenzoate, I-IV: Electron transfer chains complexes, CytC: Cytochrome C, Q: Ubiquinone, SAM: S-adenosylmethionine.

Preprints (www.preprints.org) | NOT PEER-REVIEWED | Posted: 26 August 2020 doi:10.20944/preprints202008.0580.v1

It is fatal to have defects in the biosynthesis of ubiquinone[34]. Ubiquinone is essential for electron shuttling not only from complex I (NADH ubiquinone oxidoreductase) and complex II towards complex III of mitochondrial ETC[11], but also through uncoupling proteins[35]. Ubiquinone also keeps the mitochondrial permeability transition pore closed[36]. In eukaryotes, the mitochondrial biosynthesis of ubiquinone requires mitochondrial inner membrane transport of hydroxybenzoic acid or aminobenzoic acid, which in turn are biosynthesized from L-tyrosine, L-phenylalanine, cinnamic acid, *para*-coumaric acid, or chorismate[10,36–38]. This study revealed that *Slc*25A44s co-localize with the genes coding for ETC subunits in the genome of several species (Fig. 1a, Table 1) and are involved in the transport of ubiquinone precursors, such as *para*-coumaric, hydroxybenzoic, and aminobenzoic acids. A pivotal role in respiration therefore proposed for SLC25A44s through the intracellular transport of ubiquinone precursors (Fig. 4d). This important transport activity, required for the indispensable biosynthesis of ubiquinone in higher eukaryotes, has conceivably been the main evolutionary force for the observed positive selection and the ubiquitous expression of *Slc*25A44 genes (Fig. 2c, Extended Data Table 3, Extended Data Fig. 2, 3). As an evidence for the essential function of SLC25A44, downregulation of *Slc*25A44 in *Trypanosoma brucei* led to lower levels of oxidative phosphorylation and ATP, growth arrest, and death[39]. Accordingly, the expression of SLC25A44 improved the growth rate of the PAL and TAL yeast strains (Fig. 4c). Downregulation of *Slc*25A44 in *Caenorhabditis elegans* also reduced ETC activity similar to the knockdowns in the respiratory complex I, III, and IV subunits[40]. Additionally, SLC25A44 found to be co-expressed with FOXK transcriptional regulators in mouse (Extended Data Fig. 4) and human (Extended Data Fig. 5), likely to improve the efficiency of ETC while glycolytic intermediates are mainly utilized for anabolic reactions. FOXK1 and FOXK2 favor aerobic glycolysis by uncoupling the glycolysis from mitochondrial oxidative phosphorylation[41]. It is therefore not surprising that *Slc*25A44 has the highest expression levels in human brain, kidney, and liver (Extended Data Fig. 2), which are known as the most sensitive organs to mitochondrial disorders[5,6,27] and have the highest resting metabolic rates[42]. Very recently, SLC25A44 was reported to be involved in the energy homeostasis by thermogenesis through the transport of only the branched chain amino acids (BCAAs: leucine, isoleucine, and valine) to be catabolized within mitochondria of mouse fat cells specifically and not in muscle or liver[43]. Taken together, it seems that the contribution of SLC25A44 to the metabolism of energy has evolved through both tissue-specific and common mechanisms of the BCAA transport and the ubiquinone precursor transport, respectively. This common mechanism which is introduced in this study also is in line with the SLC25A44 ubiquitous expression (Extended Data Fig. 2, 3) and positive selection (Fig. 2c, Extended Data Table 3). Additionally, SLC25A44 could play a role in the biosynthesis of flavonoids like resveratrol via subcellular distribution of cinnamic and *para*-coumaric acids. It is worth mentioning that resveratrol acts as a positive regulator of mitochondrial biogenesis and function[44]. The health-related properties of resveratrol also seem to be dependent on the interaction with quinone oxidoreductase[45]. Interestingly, the investigated gene clusters in the peanut genomes contained a gene coding for quinone oxidoreductase (Fig. 1a). Finally,

 doi:10.20944/preprints202008.0580.v1

the subcellular distribution of SLC25A44, as a mitochondrion-ER-nucleus zone transporter, seems very important for its function when considering the ER membrane encounters with mitochondrion, nucleus, and plasma membrane. This is because of the following reasons: (i) the function and structure of ubiquinone synthome is dependent on the ER-mitochondrion encounter[46]; (ii) the *para*-coumaric acid biosynthetic metabolon (including PAL and C4H but not TAL) is ER membrane-associated[33]; and finally, (iii) the flavonoid biosynthesis is associated with the ER membrane, nucleus membrane, and plasma-membrane[47]. In fact, these encounters facilitate trafficking by transporters across the engaged membranes[48].

In summary, it is revealed that SLC25A44 is involved in the energy and secondary metabolism through the transport of the common precursors for the biosynthesis of ubiquinone, flavonoids, and stilbenoids. The results also introduce the SLC25A44 ^{LWW206IQF} as a promising candidate transporter to enhance the bio-based production of *para*-coumaric acid.

Materials and Methods

DNA constructs

The integrative plasmids (Extended Data Table 4) were constructed using gene and promoter BioBricks (Extended Data Table 5). Specific primers (Extended Data Table 5) were used to amplify the fragments using Phusion U polymerase (ThermoFisher Scientific). The native genes were amplified from *S. cerevisiae* CEN.PK genomic DNA and the heterologous genes were synthetized by GeneArt. The empty integrative vectors were digested with FastDigest *SfaAI* (ThermoFisher Scientific) restriction endonuclease, nicked with *Nb.BsmI* (New England BioLabs) and finally assembled together with the PCR-amplified genes and promoters. To express the transporter coding gene in the oocytes, it was cloned downstream of the T7 promoter in the USER compatible *Xenopus* expression vector pNB1u as described previously[7,9]. The empty vector was digested by PacI and nicked by *Nt.BbvCI* (New England BioLabs) for USER-cloning of the amplified transporter ORF. The reaction was transformed into chemically competent *E. coli* cells. Finally, plasmid DNAs from single colonies were sequences and confirmed.

Yeast strain construction

All yeast strains constructed in this study are derived from CEN.PK strain[29,32] and listed in Extended Data Table 4. The native and heterologous genes under the control of strong constitutive promoters were integrated into the genome of the parental yeast strain. Before yeast transformation, the integrative vectors were linearized by FastDigest *NotI* (ThermoFisher Scientific). Yeast cells were transformed by the standard PEG/LiAc method[49]. The cells were plated on selective plates with the appropriate selection. The plates were incubated for 3-5 days.

Media and yeast cultivation conditions

Yeast cells were grown in standard YPD medium at 30°C. For selection, drop-out agar plates without leucine, uracil or histidine or a combination of these were used. Yeast strains expressing candidate transporter genes were selected by adding G418 (G8168, Sigma-Aldrich) at the final concentration of 200 µg/ml. All of the strains were confirmed for integration of the genes of interest by colony PCR using OneTaq® Hot Start Quick-Load® 2X Master Mix (New England Biolabs) using the manufacturer's protocol and primers listed in Extended Data Table 6. For production of *para*-coumaric acid, the 24 deep-well plates were used with 3-ml working volume per well. Cells from the seed cultures (in mineral medium containing 200 µg/ml of G418) were washed with sterile water, resuspended in the mineral medium to OD_{600} of 0.03. The mineral medium contained 7.5 g/l $(NH4)_2SO_4$, 14.4 g/l KH_2PO_4, 0.5 g/l $MgSO_4 \cdot 7H_2O$, 1 ml/l of vitamin solution, 2 ml/l trace elements, and 20 g/l glucose[29]. The pH was set to 6 (using 2N NaOH) before filter sterilization. The experiment was carried out with three replicates per strain. Incubation of strains at 30°C was for 72 hours and with 300-rpm agitation. After OD measurement, sample collection from yeast cultures was performed by adding 1:1 vol. 99.9% ethanol to solubilize the secreted compounds in the fermentation broth. This followed by centrifugation at 2000 g for 2 minutes to exclude the yeast cells. The supernatants were filtered through Whatman 0.45 µm PTFE membrane (CAT: 6784-0404, Life Sciences) before analysis. To measure the doubling times, yeast strains from overnight cultures were aerobically cultivated ($OD_{600} \approx 0.4$) using

YPD medium and 24 deep-well plates with 2-ml working volume at 30°C and 300-rpm agitation. Logarithmic cell growth was measured spectrophotometrically at A_{600} nm. ODs for T_1 and T_2 were measured after two and six hours, respectively. Doubling time was measured as a function of $[T_2 - T_{1\,(hours)}]/[(OD_{600},t_2 / OD_{600},t_1)^{1/2}]$.

Transport assays in *Xenopus* oocytes

The *Xenopus laevis* oocytes were obtained from Ecocyte Bioscience (Germany) and kept at 18°C. Linear cassette including T7 promoter, *AdSlc*25A44 ORF, and 3′UTR was amplified with Phusion Hot Start polymerase (ThermoFisher Scientific) and used as template for *in-vitro* transcription. Capped complementary RNAs were synthesized using the mMESSAGE mMACHINE® T7 transcription kit (AM1344; ThermoFisher). The quality and quantity of the cRNA was determined using Agilent 2100 Bioanalyzer. For expression, oocytes were kept 3 days after microinjection of 25 ng *in-vitro* transcribed cRNA of the transporter[7]. Instead of RNA, water was injected into the control oocytes, *i.e.*, with no heterologous transporter. RoboInject (Multi Channel Systems, GmbH) was used for microinjection of cRNAs and compounds[9]. In all of experiments the injection needles (Multi Channel Systems, MCS GmbH) with opening of 25 µm were used. For efflux assay, the stock solution of 10 nl containing 200 mM resveratrol and 200 mM *para*-coumaric acid was used for microinjection into the oocytes with and without the heterologous transporter to obtain an estimated internal concentration of 2 mM assuming 100X dilution after injection[7]. Following four washing steps, batches with 20 oocytes in each were incubated for 210 min in 90 µl Kulori buffer, pH 5. After incubation, 80 µl of the medium was collected from each batch with intact oocytes and added onto 60 µl of 100% MeOH before LC-MS analysis. The oocyte samples with 30 oocytes per replicate, after feeding with resveratrol and *para*-coumaric acid (200 µM each) or with cinnamic acid and 4-aminobenzoic acid (200 µM each) in Kulori buffer (pH 5) for 210 min, were washed 4 times with Kulori buffer (pH 7) and oocyte extracts were prepared in 90 µl of 60% MeOH. Finally, 30 µl water was added before analysis[7]. Statistical significant differences were determined through Student's t-test.

Chemicals and HPLC/LC-MS analyses

Resveratrol (34092) was obtained from Fluka and *trans para*-coumaric acid (C0393) was obtained from TCI. *Trans* cinnamic acid (C80857), hydroxybenzoic acid (H20059), and aminobenzoic acids (A9878) were obtained from Sigma-Aldrich. LC-MS was applied to analyze the concentrations of resveratrol and *para*-coumaric acid in the samples. LC-MS measurements were carried out on a Dionex UltiMate 3000 UHPLC (Thermo Fisher Scientific, San Jose, CA) connected to an Orbitrap Fusion Mass Spectrometer (Thermo Fisher Scientific, San Jose, CA) and using a Hypersil GOLD PFP, 15 cm × 2.1 mm, 3 µm column[29]. To quantify cinnamic acid, 4-hydroxybenzoic acid, and 4-aminobenzoic acid, 10 µl of each sample was analyzed using Dionex Ultimate 3000 HPLC with a Zorbax Eclipse Plus C18 4.6 × 100 mm, 3.5 µm (Agilent 959961-902) column and a DAD-3000 Diode Array Detector at 280 nm (Dionex). The mobile phase consisted of 0.05% acetic acid (A) and acetonitrile (B). The flow rate was 1 ml/min and the column was kept at 30°C. The mobile phase was introduced as a gradient of 5% to 12% B in 1.5 minute and was held at this composition for an additional minute. The gradient was then ramped to 30% B in 2 minutes and this gradient was held for an additional minute which followed by a linear gradient to 70% B in 2.5 minutes. This composition was kept for half minute and then changed to 5% B during 9.5 minutes. Column was equilibrated with 5% B until 11 minutes. Samples were held at 5°C during the analysis.

Bioinformatics and polymorphism analysis

The Botany Array Resource[50] and COEXPEDIA[51] were used for co-expression analysis in *A. thaliana* and mouse. Pathway enrichment was performed using the Metascape[52]. The *Arabidopsis* Genome Encyclopedia[53] (http://rarge-v2.psc.riken.jp/), TAIR and its associated Salk SNP database[54] (https://www.arabidopsis.org/), and Gramene Release 39[55] (http://www.gramene.org/) were used for inspection of the *Slc*25A44 polymorphism in *A. thaliana* which is a self-pollinating homozygote plant. The human allele database including HapMap genotypes[56] (http://bioinfo.ut.ee/HAD/) and the dbSNP Entrez data (https://www.ncbi.nlm.nih.gov/SNP/) were used to examine the polymorphism of human *Slc*25A44 locus. Three dimensional structure of *Ad*SLC25A44 was built using the Phyre2[57]. The maximum likelihood phylogenetic trees were built on the WAG substitutional matrix-based model for amino acid sequences and a bootstrap value of 1000.

Acknowledgments

The author thanks Mette Kristensen for support with analytics.

Ethics approval and consent to participate

Not applicable.

Competing interests

The author declares no competing interests.

Additional information

Supplementary information is available for this paper.

References

1. Darbani, B., Kell, D. B. & Borodina, I. Energetic evolution of cellular Transportomes. *BMC Genomics* **19,** 418 (2018).
2. Leroch, M., Neuhaus, H. E., Kirchberger, S., Zimmermann, S., Melzer, M., Gerhold, J. & Tjaden, J. Identification of a novel adenine nucleotide transporter in the endoplasmic reticulum of Arabidopsis. *Plant Cell* **20,** 438–451 (2008).
3. Palmieri, L., Rottensteiner, H., Girzalsky, W., Scarcia, P., Palmieri, F. & Erdmann, R. Identification and functional reconstitution of the yeast peroxisomal adenine nucleotide transporter. *EMBO J.* **20,** 5049–5059 (2001).
4. Weber, A. P. M., Schwacke, R. & Flügge, U.-I. Solute transporters of the plastid envelope membrane. *Annu Rev Plant Biol* **56,** 133–164 (2005).
5. Palmieri, F. The mitochondrial transporter family SLC25: identification, properties and physiopathology. *Mol. Aspects Med.* **34,** 465–484 (2013).
6. Wallace, D. C. Mitochondrial Diseases in Man and Mouse. *Science* **283,** 1482–1488 (1999).
7. Darbani, B., Motawia, M. S., Olsen, C. E., Nour-Eldin, H. H., Møller, B. L. & Rook, F. The biosynthetic gene cluster for the cyanogenic glucoside dhurrin in *Sorghum bicolor* contains its co-expressed vacuolar MATE transporter. *Scientific Reports* **6,** 37079 (2016).
8. Wierckx, N., Agrimi, G., Lübeck, P. S., Steiger, M. G., Mira, N. P. & Punt, P. J. Metabolic specialization in itaconic acid production: a tale of two fungi. *Curr. Opin. Biotechnol.* **62,** 153–159 (2019).
9. Darbani, B., Stovicek, V., Hoek, S. A. van der & Borodina, I. Engineering energetically efficient transport of dicarboxylic acids in yeast Saccharomyces cerevisiae. *PNAS* 201900287 (2019). doi:10.1073/pnas.1900287116
10. Threlfall, D. R., Law, A. & Whistance, G. R. Cinnamic acid and p-coumaric acid, precursors of ubiquinone in higher plants, green algae and fungi. *Biochem. J.* **118,** 55P (1970).
11. Crane, F. L., Hatefi, Y., Lester, R. L. & Widmer, C. Isolation of a quinone from beef heart mitochondria. *Biochim. Biophys. Acta* **25,** 220–221 (1957).
12. Zhang, X. & Liu, C.-J. Multifaceted Regulations of Gateway Enzyme Phenylalanine Ammonia-Lyase in the Biosynthesis of Phenylpropanoids. *Molecular Plant* **8,** 17–27 (2015).
13. Takos, A. M. & Rook, F. Why biosynthetic genes for chemical defense compounds cluster. *Trends in Plant Science* **17,** 383–388 (2012).
14. Sweetman, C., Wong, D. C., Ford, C. M. & Drew, D. P. Transcriptome analysis at four developmental stages of grape berry (Vitis vinifera cv. Shiraz) provides insights into regulated and coordinated gene expression. *BMC Genomics* **13,** 691 (2012).
15. Agrimi, G., Di Noia, M. A., Marobbio, C. M. T., Fiermonte, G., Lasorsa, F. M. & Palmieri, F. Identification of the human mitochondrial S-adenosylmethionine transporter: bacterial expression, reconstitution, functional characterization and tissue distribution. *Biochem. J.* **379,** 183–190 (2004).
16. Shaw, G. C., Cope, J. J., Li, L., Corson, K., Hersey, C., Ackermann, G. E., Gwynn, B., Lambert, A. J., Wingert, R. A., Traver, D., Trede, N. S., Barut, B. A., Zhou, Y., Minet, E., Donovan, A., Brownlie, A., Balzan, R., Weiss, M. J., Peters, L. L., Kaplan, J., Zon, L. I. & Paw, B. H. Mitoferrin is essential for erythroid iron assimilation. *Nature* **440,** 96–100 (2006).
17. Guernsey, D. L., Jiang, H., Campagna, D. R., Evans, S. C., Ferguson, M., Kellogg, M. D., Lachance, M., Matsuoka, M., Nightingale, M., Rideout, A., Saint-Amant, L., Schmidt, P. J., Orr, A., Bottomley, S. S., Fleming, M. D., Ludman, M., Dyack, S., Fernandez, C. V. & Samuels, M. E. Mutations in mitochondrial carrier family gene SLC25A38 cause nonsyndromic autosomal recessive congenital sideroblastic anemia. *Nat. Genet.* **41,** 651–653 (2009).
18. Nilsson, R., Schultz, I. J., Pierce, E. L., Soltis, K. A., Naranuntarat, A., Ward, D. M., Baughman, J. M., Paradkar, P. N., Kingsley, P. D., Culotta, V. C., Kaplan, J., Palis, J., Paw, B. H. & Mootha, V. K. Discovery of genes essential for heme biosynthesis through large-scale gene expression analysis. *Cell Metab.* **10,** 119–130 (2009).
19. Kishita, Y., Pajak, A., Bolar, N. A., Marobbio, C. M. T., Maffezzini, C., Miniero, D. V., Monné, M., Kohda, M., Stranneheim, H., Murayama, K., Naess, K., Lesko, N., Bruhn, H., Mourier, A., Wibom, R., Nennesmo, I., Jespers, A., Govaert, P., Ohtake, A., Van Laer, L., Loeys, B. L., Freyer, C., Palmieri, F., Wredenberg, A., Okazaki, Y. & Wedell, A. Intra-mitochondrial Methylation Deficiency Due to Mutations in SLC25A26. *The American Journal of Human Genetics* **97,** 761–768 (2015).
20. Kim, H. J., Khalimonchuk, O., Smith, P. M. & Winge, D. R. Structure, function, and assembly of heme centers in mitochondrial respiratory complexes. *Biochim. Biophys. Acta* **1823,** 1604–1616 (2012).
21. Darbani, B., Briat, J.-F., Holm, P. B., Husted, S., Noeparvar, S. & Borg, S. Dissecting plant iron homeostasis under short and long-term iron fluctuations. *Biotechnology Advances* **31,** 1292–1307 (2013).
22. Darbani, B., Noeparvar, S. & Borg, S. Deciphering Mineral Homeostasis in Barley Seed Transfer Cells at Transcriptional Level. *PLoS ONE* **10,** e0141398 (2015).
23. Uhlen, M., Oksvold, P., Fagerberg, L., Lundberg, E., Jonasson, K., Forsberg, M., Zwahlen, M., Kampf, C., Wester, K., Hober, S., Wernerus, H., Björling, L. & Ponten, F. Towards a knowledge-based Human Protein Atlas. *Nat. Biotechnol.* **28,** 1248–1250 (2010).
24. Baerenfaller, K., Grossmann, J., Grobei, M. A., Hull, R., Hirsch-Hoffmann, M., Yalovsky, S., Zimmermann, P., Grossniklaus, U., Gruissem, W. & Baginsky, S. Genome-Scale Proteomics Reveals Arabidopsis thaliana Gene Models and Proteome Dynamics. *Science* **320,** 938–941 (2008).
25. Schmid, M., Davison, T. S., Henz, S. R., Pape, U. J., Demar, M., Vingron, M., Schölkopf, B., Weigel, D. & Lohmann, J. U. A gene expression map of Arabidopsis thaliana development. *Nat. Genet.* **37,** 501–506 (2005).
26. He, Y.-N., Peng, J.-S., Cai, Y., Liu, D.-F., Guan, Y., Yi, H.-Y. & Gong, J.-M. Tonoplast-localized nitrate uptake transporters involved in vacuolar nitrate efflux and reallocation in Arabidopsis. *Scientific Reports* **7,** 6417 (2017).
27. Gutiérrez-Aguilar, M. & Baines, C. P. Physiological and pathological roles of mitochondrial SLC25 carriers. *Biochem. J.* **454,** 371–386 (2013).
28. Huh, W.-K., Falvo, J. V., Gerke, L. C., Carroll, A. S., Howson, R. W., Weissman, J. S. & O'Shea, E. K. Global analysis of protein localization in budding yeast. *Nature* **425,** 686–691 (2003).

29. Li, M., Schneider, K., Kristensen, M., Borodina, I. & Nielsen, J. Engineering yeast for high-level production of stilbenoid antioxidants. *Sci Rep* **6,** 36827 (2016).
30. Marbois, B., Xie, L. X., Choi, S., Hirano, K., Hyman, K. & Clarke, C. F. *para* -Aminobenzoic Acid Is a Precursor in Coenzyme Q_6 Biosynthesis in *Saccharomyces cerevisiae*. *Journal of Biological Chemistry* **285,** 27827–27838 (2010).
31. Payet, L.-A., Leroux, M., Willison, J. C., Kihara, A., Pelosi, L. & Pierrel, F. Mechanistic Details of Early Steps in Coenzyme Q Biosynthesis Pathway in Yeast. *Cell Chemical Biology* **23,** 1241–1250 (2016).
32. Rodriguez, A., Kildegaard, K. R., Li, M., Borodina, I. & Nielsen, J. Establishment of a yeast platform strain for production of p-coumaric acid through metabolic engineering of aromatic amino acid biosynthesis. *Metabolic Engineering* **31,** 181–188 (2015).
33. Achnine, L., Blancaflor, E. B., Rasmussen, S. & Dixon, R. A. Colocalization of L-phenylalanine ammonia-lyase and cinnamate 4-hydroxylase for metabolic channeling in phenylpropanoid biosynthesis. *Plant Cell* **16,** 3098–3109 (2004).
34. Wang, Y., Oxer, D. & Hekimi, S. Mitochondrial function and lifespan of mice with controlled ubiquinone biosynthesis. *Nat Commun* **6,** 6393 (2015).
35. Echtay, K. S., Winkler, E., Frischmuth, K. & Klingenberg, M. Uncoupling proteins 2 and 3 are highly active H+ transporters and highly nucleotide sensitive when activated by coenzyme Q (ubiquinone). *Proc Natl Acad Sci U S A* **98,** 1416–1421 (2001).
36. Turunen, M., Olsson, J. & Dallner, G. Metabolism and function of coenzyme Q. *Biochimica et Biophysica Acta (BBA) - Biomembranes* **1660,** 171–199 (2004).
37. Stefely, J. A. & Pagliarini, D. J. Biochemistry of Mitochondrial Coenzyme Q Biosynthesis. *Trends Biochem Sci* **42,** 824–843 (2017).
38. Pierrel, F. Impact of Chemical Analogs of 4-Hydroxybenzoic Acid on Coenzyme Q Biosynthesis: From Inhibition to Bypass of Coenzyme Q Deficiency. *Front Physiol* **8,** 436 (2017).
39. de Macêdo, J. P., Schumann Burkard, G., Niemann, M., Barrett, M. P., Vial, H., Mäser, P., Roditi, I., Schneider, A. & Bütikofer, P. An Atypical Mitochondrial Carrier That Mediates Drug Action in Trypanosoma brucei. *PLOS Pathogens* **11,** e1004875 (2015).
40. Yanos, M. E., Bennett, C. F. & Kaeberlein, M. Genome-Wide RNAi Longevity Screens in Caenorhabditis elegans. *Curr. Genomics* **13,** 508–518 (2012).
41. Sukonina, V., Ma, H., Zhang, W., Bartesaghi, S., Subhash, S., Heglind, M., Foyn, H., Betz, M. J., Nilsson, D., Lidell, M. E., Naumann, J., Haufs-Brusberg, S., Palmgren, H., Mondal, T., Beg, M., Jedrychowski, M. P., Taskén, K., Pfeifer, A., Peng, X.-R., Kanduri, C. & Enerbäck, S. FOXK1 and FOXK2 regulate aerobic glycolysis. *Nature* **566,** 279–283 (2019).
42. Müller, M. J., Wang, Z., Heymsfield, S. B., Schautz, B. & Bosy-Westphal, A. Advances in the understanding of specific metabolic rates of major organs and tissues in humans. *Curr Opin Clin Nutr Metab Care* **16,** 501–508 (2013).
43. Yoneshiro, T., Wang, Q., Tajima, K., Matsushita, M., Maki, H., Igarashi, K., Dai, Z., White, P. J., McGarrah, R. W., Ilkayeva, O. R., Deleye, Y., Oguri, Y., Kuroda, M., Ikeda, K., Li, H., Ueno, A., Ohishi, M., Ishikawa, T., Kim, K., Chen, Y., Sponton, C. H., Pradhan, R. N., Majd, H., Greiner, V. J., Yoneshiro, M., Brown, Z., Chondronikola, M., Takahashi, H., Goto, T., Kawada, T., Sidossis, L., Szoka, F. C., McManus, M. T., Saito, M., Soga, T. & Kajimura, S. BCAA catabolism in brown fat controls energy homeostasis through SLC25A44. *Nature* **572,** 614–619 (2019).
44. Jardim, F. R., de Rossi, F. T., Nascimento, M. X., da Silva Barros, R. G., Borges, P. A., Prescilio, I. C. & de Oliveira, M. R. Resveratrol and Brain Mitochondria: a Review. *Mol Neurobiol* **55,** 2085–2101 (2018).
45. Buryanovskyy, L., Fu, Y., Boyd, M., Ma, Y., Hsieh, T., Wu, J. M. & Zhang, Z. Crystal structure of quinone reductase 2 in complex with resveratrol. *Biochemistry* **43,** 11417–11426 (2004).
46. Eisenberg-Bord, M., Tsui, H. S., Antunes, D., Fernández-del-Río, L., Bradley, M. C., Dunn, C. D., Nguyen, T. P. T., Rapaport, D., Clarke, C. F. & Schuldiner, M. The Endoplasmic Reticulum-Mitochondria Encounter Structure Complex Coordinates Coenzyme Q Biosynthesis. *Contact* **2,** 2515256418825409 (2019).
47. Fornara, V., Onelli, E., Sparvoli, F., Rossoni, M., Aina, R., Marino, G. & Citterio, S. Localization of stilbene synthase in Vitis vinifera L. during berry development. *Protoplasma* **233,** 83–93 (2008).
48. Phillips, M. J. & Voeltz, G. K. Structure and function of ER membrane contact sites with other organelles. *Nature Reviews Molecular Cell Biology* **17,** 69–82 (2016).
49. Gietz, R. D. & Woods, R. A. Yeast transformation by the LiAc/SS Carrier DNA/PEG method. *Methods Mol. Biol.* **313,** 107–120 (2006).
50. Toufighi, K., Brady, S. M., Austin, R., Ly, E. & Provart, N. J. The Botany Array Resource: e-Northerns, Expression Angling, and promoter analyses. *Plant J.* **43,** 153–163 (2005).
51. Yang, S., Kim, C. Y., Hwang, S., Kim, E., Kim, H., Shim, H. & Lee, I. COEXPEDIA: exploring biomedical hypotheses via co-expressions associated with medical subject headings (MeSH). *Nucleic Acids Res.* **45,** D389–D396 (2017).
52. Zhou, Y., Zhou, B., Pache, L., Chang, M., Khodabakhshi, A. H., Tanaseichuk, O., Benner, C. & Chanda, S. K. Metascape provides a biologist-oriented resource for the analysis of systems-level datasets. *Nat Commun* **10,** 1–10 (2019).
53. Akiyama, K., Kurotani, A., Iida, K., Kuromori, T., Shinozaki, K. & Sakurai, T. RARGE II: an integrated phenotype database of Arabidopsis mutant traits using a controlled vocabulary. *Plant Cell Physiol.* **55,** e4 (2014).
54. Lamesch, P., Berardini, T. Z., Li, D., Swarbreck, D., Wilks, C., Sasidharan, R., Muller, R., Dreher, K., Alexander, D. L., Garcia-Hernandez, M., Karthikeyan, A. S., Lee, C. H., Nelson, W. D., Ploetz, L., Singh, S., Wensel, A. & Huala, E. The Arabidopsis Information Resource (TAIR): improved gene annotation and new tools. *Nucleic Acids Res* **40,** D1202–D1210 (2012).
55. Youens-Clark, K., Buckler, E., Casstevens, T., Chen, C., Declerck, G., Derwent, P., Dharmawardhana, P., Jaiswal, P., Kersey, P., Karthikeyan, A. S., Lu, J., McCouch, S. R., Ren, L., Spooner, W., Stein, J. C., Thomason, J., Wei, S. & Ware, D. Gramene database in 2010: updates and extensions. *Nucleic Acids Res.* **39,** D1085-1094 (2011).
56. International HapMap 3 Consortium, Altshuler, D. M., Gibbs, R. A., Peltonen, L., Altshuler, D. M., Gibbs, R. A., Peltonen, L., Dermitzakis, E., Schaffner, S. F., Yu, F., Peltonen, L., Dermitzakis, E., Bonnen, P. E., Altshuler, D. M., Gibbs, R. A., de Bakker, P. I. W., Deloukas, P., Gabriel, S. B., Gwilliam, R., Hunt, S., Inouye, M., Jia, X., Palotie, A., Parkin, M., Whittaker, P., Yu, F., Chang, K., Hawes, A., Lewis, L. R., Ren, Y., Wheeler, D., Gibbs, R. A., Muzny, D. M., Barnes, C., Darvishi, K., Hurles, M., Korn, J. M., Kristiansson, K., Lee, C., McCarrol, S. A., Nemesh, J., Dermitzakis, E., Keinan, A., Montgomery, S. B., Pollack, S., Price, A. L., Soranzo, N., Bonnen, P. E., Gibbs, R. A., Gonzaga-Jauregui, C., Keinan, A., Price, A. L., Yu, F., Anttila, V., Brodeur, W., Daly, M. J., Leslie, S., McVean, G., Moutsianas, L., Nguyen, H., Schaffner, S. F., Zhang, Q., Ghori, M. J. R., McGinnis, R., McLaren, W., Pollack, S., Price, A. L., Schaffner, S. F., Takeuchi, F., Grossman, S. R., Shlyakhter, I., Hostetter, E. B., Sabeti, P. C., Adebamowo, C. A., Foster, M. W., Gordon, D. R., Licinio, J., Manca, M. C., Marshall, P. A., Matsuda, I., Ngare, D., Wang, V. O., Reddy, D., Rotimi, C. N., Royal, C. D., Sharp, R. R., Zeng, C., Brooks, L. D. & McEwen, J. E. Integrating common and rare genetic variation in diverse human populations. *Nature* **467,** 52–58 (2010).

57. Kelley, L. A., Mezulis, S., Yates, C. M., Wass, M. N. & Sternberg, M. J. E. The Phyre2 web portal for protein modeling, prediction and analysis. *Nat Protoc* **10,** 845–858 (2015).